Gold nanorods coated with a thermo-responsive poly(ethylene glycol)-b-poly(N-vinylcaprolactam) corona as drug delivery systems for remotely near infrared-triggered release

Ji Liu, Christophe Detrembleur, Marie-Claire de Pauw-Gillet, Stéphane
Mornet, Etienne Duguet, Christine Jérôme

Gold Nanorods Coated with a Thermo-responsive Poly(ethylene glycol)-*b*-poly(*N*-vinylcaprolactam) Corona as Drug Delivery Systems for Remotely Near Infrared-Triggered Release †

Ji Liu,[a,c] Christophe Detrembleur,*[a] Marie-Claire De Pauw-Gillet,[b] Stéphane Mornet,[c] Etienne Duguet *[c] and Christine Jérôme*[a]

Poly(ethylene glycol)-*b*-poly(*N*-vinylcaprolactam) (PEG-*b*-PNVCL) copolymers are prepared from a PEG macro-chain transfer agent in DMF at 65 °C via reversible addition-fragmentation chain transfer (RAFT) polymerization. Well-defined PEG$_{114}$-*b*-PNVCL$_{237}$ copolymer with a could point temperature of 39 °C is used for the formation of a thermo-responsive polymer corona on the surface of gold nanorods (GNRs) via a "grafting-to" approach. Thermo-responsiveness and thermo-dependent optical properties of the as-obtained GNR@PEG-*b*-PNVCL nanoparticles are studied with dynamic light scattering and UV/*vis* spectroscopy techniques. Near infrared (NIR)-induced heating of GNR@PEG-*b*-PNVCL is also explored in aqueous suspension under NIR laser irradiation (802 nm, up to 250 mW). The potential of these GNR@PEG-*b*-PNVCL nanoparticles to be used as smart drug delivery systems (DDS) is then studied. A hydrophilic drug model, Rhodamine® B, is used to assess the guest loading capacity, and triggered release behaviours are then evaluated under conventional external heating or internal heating induced by remote NIR irradiation. Cytotoxicity evaluation of the GNR@PEG-*b*-PNVCL against fibroblast-like L929 cell line is carried out via the MTS assay, in order to confirm the improved biocompatibility of the GNRs after polymer coating. These thermo-responsive GNR@PEG-*b*-PNVCL nanoparticles are promising DDS that combine the chemotherapeutic and phototherapeutic functions.

Introduction

Light-sensitive systems have recently received increasing interest in biomedical applications, such as drug delivery system (DDS), phototherapy, due to the high specificity, non-invasive and low toxic nature of the light stimulus.[1, 2] Similar to gold nanoshells, nanostars and nanocages, gold nanorods (GNRs) also demonstrate structure-dependent optical properties, with tuneable photothermal response to light.[3-8] In particular, two adsorption bands, transverse and longitudinal modes of surface plasmon resonance (SPR), could be observed in a typical UV/*vis* adsorption spectrum of GNRs; the former one always locates at *ca.* 520 nm, and the latter can be tuned to the visible or NIR region, depending on the aspect ratio.[2, 5, 6] This distinctive optical characteristic, combined with other properties such as biocompatibility and facile surface functionalization, opens up the fascinating applications of GNRs in the biomedical field.

Light excitation in resonance with the longitudinal SPR could heat the GNRs to a high temperature locally, other than a whole-range hyperthermia.[1, 2, 9-11] This specific heating capacity makes the GNRs appealing for tumours treatment via photothermal ablation, due to the protein denaturation from overheating (> 42 °C).[10, 12] Generally, an ideal phototherapeutic window for clinical tumours treatment is in the NIR range (650 ~ 950 nm), in which the attenuation of light by blood or other soft tissues is very low,[12, 13] allowing for a deeper penetration and targeting to deep-located compartments, such as tumours. On the other hand, due to the dependence of longitudinal SPR band on aspect ratio, it is very easy to get GNRs with SPR band in the NIR range by controlling the aspect ratio.[2, 6, 14] Thus, the capability of GNRs to generate local heating under NIR irradiation with manipulative controls (wave length, power and irradiation period) suggests significant promise for clinical tumor treatment via this kind of phototherapy. Up to now, some works have been reported on GNRs used for tumour treatment via photothermia.[9, 15-24]

In addition to the phototherapeutic application, NIR-induced heating of GNRs could also be utilized for remotely triggered-release of drugs or genes, which were usually immobilized on the surface of GNRs, uploaded in the external mesoporous silica cavities or functional polymer corona.[25-34] For the latter, due to the facile surface functionalization of GNRs, a thermo-responsive polymer corona could be easily introduced via the "grafting from" or "grafting to" strategy.[35, 36] _ENREF_36 Polymers prepared from reversible addition-fragmentation transfer (RAFT) polymerization are characterized with their ω-chain end groups, such as trithiocarbonate, dithioester or xanthate groups, which are able to strongly bind to the surface of gold nanoparticles (GNPs) via the Au-S conjugation.[37-41] Up to now, there are some reports on forming thermo-responsive corona on the surface of GNPs with poly(*N*-isopropyl acrylamide) (PNiPAAm)[39-43] or poly(*N*-vinylcaprolactam) (PNVCL)[38] homopolymer prepared via RAFT technique. However, due to the hydrophobic essence of the polymer corona above their lower critical solution temperature (LCST), such as *ca.* 32 °C for the GNPs@PNiPAAm,[44] 33-39 °C

for the GNPs@PNVCL (LCST decided by M_n of PNVCL),[38] 34 °C for the GNR@PNiPAAm,[42, 45] aggregation occurred above the LCST, resulting in un-stable dispersions. This lack of GNPs stabilization might constitute a limitation for their use in biomedical applications, especially for those with LCST below the physiological temperature (37 °C).

In this study, thermo-responsive poly(ethylene glycol)-*b*-poly(*N*-vinylcaprolactam) (PEG-*b*-PNVCL) copolymers are synthesized via RAFT polymerization from a PEG-macro chain transfer agent (CTA) (Scheme 1). PEG$_{114}$-*b*-PNVCL$_{25-237}$ copolymers with tuneable cloud point temperature (T_c) are obtained, by controlling the PNVCL block length. The as-prepared PEG-*b*-PNVCL copolymers are then immobilized onto the surface of gold nanorods (aspect ratio: 3.8, longitudinal SPR band: 795 nm) via a "grafting to" approach to form a thermo-responsive corona. The goal of this work is to develop thermo-responsive gold nanorods (GNR@PEG-*b*-PNVCL) with: (i) good stability not only under physiological conditions ($T_c > 37$ °C), but also above the T_c due to the steric-repulsion by the hydrophilic PEG blocks (Scheme 2); and (ii) potential application as DDS for remotely-triggered drug release under NIR activation. Studies on the NIR-induced heating capability of the GNR@PEG-*b*-PNVCL in aqueous suspensions are carried out with a NIR laser diode (802 nm, up to 250 mW). Model studies on guest loading capacity and remotely NIR-triggered release are tested with Rhodamine® B, a hydrophobic model drug. Cytotoxicity of the as-prepared GNR@PEG-*b*-PNVCL against mouse fibroblast-like L929 cell line is also evaluated via the MTS assay.

Experimental Details

Materials

Poly(ethylene glycol) methyl ether (mPEG$_{114}$-OH, M_n 5000 g/mol), triethylamine (TEA, 99.5%), pyridine (99%), 2-bromopropionyl bromide (97%), potassium ethyl xanthogenate (96%), 2, 2′-azobis(2-methylpropionitrile) (AIBN, 98%), ascorbic acid (AA, 98%), cetyltrimethylammonium bromide (CTAB, 99%), silver nitric (AgNO$_3$, 99%), tetrachloroauric acid trihydrate (HAuCl$_4$·3H$_2$O, 99.9%), sodium borohydride (NaBH$_4$, 99%), sodium hydroxide (NaOH, 98.5%), sodium phosphate dibasic (Na$_2$HPO$_4$, 98%), potassium phosphate monobasic (KH$_2$PO$_4$, 98%), Rhodamine® B (RB, 95%), hydrochloric acid (HCl, 37%), hydrofluoric acid (HF, 48 *wt*.%), sulfuric acid (H$_2$SO$_4$, 98%), fluorescein isothiocyanate isomer I (FITC, 90%), potassium chloride (KCl, 99%) and 4′, 6′-diamidino-2-phenylindole (DAPI, 98%) were purchased from *Aldrich/Sigma*. 3-(4,5-dimethyl-thiazol-2-yl)-5-(3-carboxymethoxyphenyl)-2-(4-sulfophenyl)-2H-tetrazolium (MTS) was purchased from *Promega* (Madison, USA). Dulbecco's modified Eagle medium (DMEM, glucose 1 g/L), *L*-glutamine, PBS buffer solution (Ca^{2+} and Mg^{2+} free), fetal bovine serum (FBS) and trypsin were obtained from Biowhittaker (Walkersville, MD). PBS buffer solution (with Ca^{2+} and Mg^{2+}), penicillin G, and streptomycin were purchased from GIBCO BRL (Gaithersburg, MD). *N*-vinylcaprolactam (NVCL, 98%, Aldrich) monomers were dissolved in dry dimethylformamide (NVCL/DMF = 1/3 *wt*./*vol*.%), degassed by 30-min argon bubbling and then dried with molecular sieves.

Methods

Preparation of mPEG macro-chain transfer agent (macro-CTA)

The mPEG macro-CTA was prepared from poly(ethylene glycol) methyl ether (mPEG$_{114}$-OH) using a two-step procedure as shown in Scheme 1.

In the first-step, mPEG$_{114}$-OH (20 g, 4 mmol -OH group) and triethylamine (TEA, 1.67 mL, 12 mmol) in a 250-mL round-bottom flask were mixed with 100 mL of anhydrous CH$_2$Cl$_2$ in an ice bath. A solution of 2-bromopropionyl bromide (1.3 mL, 12 mmol) in anhydrous CH$_2$Cl$_2$ (20 mL) was added drop-wise to the solution over 2 h. The solution was then allowed to warm to room temperature and was stirred for 24 h. After removal of the precipitate by filtration, 300 mL of CH$_2$Cl$_2$ were added, and the organic solution was washed successively with 1.0 M HCl solution (3 × 50 mL), 1.0 M NaOH solution (3 × 50 mL) and de-ionized water (2 × 50 mL), and then dried with anhydrous MgSO$_4$. The polymer solution was concentrated in a rotary evaporator to *ca*. 20 mL and then precipitated into 150 mL of cold diethyl ether. The product was dried overnight under vacuum at 30 °C leading to mPEG$_{114}$-Br (18.9 g. 92% yield). ^{1}H NMR (250 MHz. CDCl$_3$. δ): 4.36 (q, 1H, C*H*Br), 4.28, (m, 2H, CH$_2$C*H$_2$*OC(O)), 3.5~3.8 (m, -C*H$_2$*C*H$_2$*O- of PEG backbones), 3.34 (s. 3H, C*H$_3$*OCH$_2$CH$_2$O), 1.79 (d, 3H, CHC*H$_3$*) (see ESI, Fig. S1a†). M_n of 8,330 g/mol (eq. PS) and M_w/M_n of 1.02 were determined by SEC in THF (see ESI, Fig. S1b†).

In the second step, mPEG$_{114}$-Br (10.3 g, 2 mmol) was dissolved in acetone (100 mL) in a 250-mL round-bottom flask and mixed with pyridine (2 mL, 10 mmol). Potassium ethyl xanthogenate (0.64 g, 4 mmol) in 20 mL of acetone was added drop-wise. The mixture was then stirred at room temperature for 24 h. After removal of the precipitate by filtration and acetone with a rotary evaporator, the crude product was dissolved in 200 mL of CH$_2$Cl$_2$. The organic solution was washed successively with 1.0 M HCl solution (3 × 30 mL), 1.0 M NaOH solution (3 × 30 mL) and de-ionized water (2 × 30 mL), and then dried with anhydrous MgSO$_4$. The polymer solution was concentrated to *ca*. 20 mL with a rotary evaporator, and then precipitated into 150 mL of cold diethyl ether and dried overnight under vacuum at 30 °C. mPEG$_{114}$-X was obtained (9.7 g, 94% yield). ^{1}H NMR (250 MHz. CDCl$_3$. δ): 4.62 (q, 2H, SC(S)OC*H$_2$*CH$_3$), 4.36 (q, 1H, C*H*Br), 4.28, (m, 2H, CH$_2$C*H$_2$*OC(O)). 3.5~3.8 (m. -C*H$_2$*C*H$_2$*O- of PEG backbones), 3.34 (s, 3H, C*H$_3$*OCH$_2$CH$_2$O), 1.56 (d, 3H, CHC*H$_3$*) 1.40 (t, 3H, SC(S)OCH$_2$C*H$_3$*) (see ESI, Fig. S1a†). M_n of 8,520 g/mol (eq. PS), M_w/M_n of 1.02 were determined by SEC analysis in THF (see ESI, Fig. S1b†).

Preparation of poly(ethylene glycol)-*b*-poly(*N*-vinylcaprolactam) block copolymers (PEG-*b*-PNVCL)

In a typical RAFT polymerization, mPEG$_{114}$-X macro-CTA (104 mg, 0.2 mmol) and AIBN (6.6 mg, 0.04 mmol) were added into a 50-mL round-bottom flask capped with a three-way stopcock. The mixture was dried via azeotropic distillation of toluene (25 mL × 2) under reduced pressure with a room-temperature water bath. After purging by three vacuum-argon cycles, a solution of NVCL monomer (5.6 g, 90 mmol) in DMF (NVCL/DMF = 1/3 *wt*./*vol*.%) was added ([M$_0$]/[I]/[CTA] of 200/0.2/1), and then the mixture was stirred at 65 ºC. Samples were periodically withdrawn with a syringe, and immediately quenched with liquid nitrogen. Monomer conversions of the PEG-*b*-PNVCL copolymers were determined

by ^{1}H NMR spectroscopy, while molecular weight (M_n) and molecular weight distribution (M_w/M_n) by SEC analysis in THF. When the NVCL conversion reached *ca.* 34.4% after 14 h, the reaction was stopped by cooling rapidly the flask to room temperature with liquid nitrogen. The final PEG-b-PNVCL copolymer was precipitated into 150 mL of cold diethyl ether and then dissolved in THF again. This purification procedure was repeated again before drying overnight under vacuum at 30 °C. The chemical composition of PEG$_{114}$-b-PNVCL$_{59}$ was confirmed by ^{1}H NMR spectroscopy (CDCl$_3$, Fig. 1a). M_n of 12,100 g/mol (eq. PS) and M_w/M_n of 1.04 were determined by SEC analysis in THF (Table 1, entry 2). PEG-b-PNVCL copolymers with other compositions were also prepared following the same protocol with different [M$_0$]/[I]/[CTA] feeding ratios and monomer conversions (Table 1).

Preparation of gold nanorods (GNRs)

Gold nanorods were prepared via the well-established seed-mediated growth method,[14] with some minor modifications.

First, CTAB-coated gold seeds (< 4 nm) were prepared via the chemical reduction of HAuCl$_4$ with NaBH$_4$. In a typical procedure, 0.25 mL of HAuCl$_4$ solution (10 mM) was mixed with 7.5 mL of CTAB solution (100 mM) in a 25-mL round-bottom flask under stirring. Then, 0.6 mL of ice-cold NaBH$_4$ solution (10 mM) was injected quickly under vigorous stirring, immediately the solution turned brown-yellow, suggesting the formation of gold seeds. It is deserved to note that the gold seeds dispersion was stored for 6 h before further use, to allow the complete decomposition of excess NaBH$_4$.

Secondly, the GRNs were prepared from gold seeds within the growth solution. Specifically, a growth solution containing 100 mL of CTAB solution (100 mM), 5 mL of HAuCl$_4$ solution (10 mM), 1 mL of AgNO$_3$ solution (10 mM) and 1 mL of H$_2$SO$_4$ (1 M) was poured into a 250-mL round-bottom flask and equilibrated at 30 °C under stirring for 30 min, then 0.8 mL of ascorbic acid (100 mM) was injected quickly under vigorous stirring, immediately the solution became colourless. Then, 250 μL of gold seeds dispersion from the first step was added under vigorous stirring for 2 min and then left un-disturbed for 6 h. The as-prepared GNRs were purified via centrifugation (12,000 rpm for 15 min) and dispersion in 40 mL of de-ionized water. Averaged size was confirmed to be *ca.* 18 ± 4 nm in width and 69 ± 8 nm in length from TEM observation (see ESI, Fig. S2†), *i.e.* an estimated aspect ratio of *ca.* 3.8. The GNRs also exhibited a longitudinal surface plasma resonance (SPR) band at *ca.* 795 nm in its UV/*vis* spectrum (see ESI, Fig. S4a†), and GNRs concentration of *ca.* 1.14 mM via ICP/OES analysis, namely, *ca.* 7.2 × 10^8 GNRs/mL was estimated.

Preparation of GNR@PEG-*b*-PNVCL nanoparticles

As reported, the GNRs prepared via the seed-mediated growth method were capped with a bi-layer of CTAB, with a positively-charged surface.[46] In order to replace CTAB with PEG-b-PNVCL, 10 mL of the original GNRs suspension was centrifuged again (12,000 rpm for 15 min) to remove the extra free CTAB, and then mixed with 5 mL of PEG-b-PNVCL aqueous solution (0.1 g/L) under stirring overnight. The extra free macromolecules were eliminated by two centrifugation/rinsing cycles (7,000 rpm for 10 min), and the GNR@PEG-b-PNVCL were re-dispersed in de-ionized water or PBS buffer solution (10 mM) under 2-min

sonication. Polymer fraction of *ca.* 12 *wt.* % was confirmed by TGA (Fig. 4b), and surface of the GNRs changed from positively-charged (ζ of +35.6 mV, pH of 7.4) to nearly neutral (ζ of -5.1 mV, pH of 7.4) after polymer coating.

Model studies on guest loading and triggered release behaviours of the GNR@PEG-*b*-PNVCL as DDS

5 mL of GNR@PEG-b-PNVCL (0.5 g/L) in PBS buffer solution (pH of 7.4) were mixed with 0.2 mL of Rhodamine® B (RB)/PBS solution (1 g/L). After stirring overnight, the RB-loaded GNR@PEG-b-PNVCL nanoparticles were purified by two centrifugation/rinsing cycles (7,000 rpm for 5 min), and then re-dispersed in PBS (10 mM, pH of 7.4) buffer solution. The centrifugation supernatants were collected to estimate the drug loading amount with its UV/*vis* absorbance at 555 nm, thanks to the pre-determined calibration curve. Drug loading capacity (*DLC*) and drug loading efficiency (*DLE*) were calculated according to the following equations:

$$DLC\% = \frac{mass\ of\ RB\ loaded}{mass\ of\ GNR@PEG\text{-}b\text{-}PNVCL} \quad (1)$$

$$DLE\% = \frac{mass\ of\ RB\ loaded}{mass\ of\ RB\ fed} \quad (2)$$

Release profiles of the RB-loaded GNR@PEG-b-PNVCL were studied via the conventional dialysis strategy. 1.5 mL of RB-loaded GNR@PEG-b-PNVCL aqueous suspension was sealed in a dialysis bag (cut-off: 2,000 g/mol), and then dialyzed against 5 mL of PBS buffer solution (10 mM, pH 7.4) under gentle stirring at different temperatures. At each pre-determined interval, 0.2 mL of the release medium solution was withdrawn, and its UV/*vis* absorbance at 555 nm was used to quantify the amount of RB released with the pre-determined calibration curve, while 0.2 mL of fresh PBS buffer solution were added to keep the volume constant. All the release profiles were presented in a cumulative mode (Fig. 8b), and the bar graphs in the figures were represented as mean values (± standard deviation) from three independent experiments.

NIR-induced heating profiles and remotely NIR-triggered release

Studies on the light-induced heating behaviours of the GNR@PEG-b-PNVCL in aqueous suspension was performed with a laser diode (802 nm, Laser 2000) with output power in the range of 0-250 mW. An Eppendorf tube, with the cap opened, was filled with the GNR@PEG-b-PNVCL aqueous suspension (1.5 mL) with a known concentration, and then fixed inside a formed plastic as insulating layer (see ESI, Fig. S3†). The laser diode was set 0.5 cm above the liquid surface. Upon the application of NIR irradiation with different powers, evolution of temperatures of the GNR@PEG-b-PNVCL aqueous suspension was monitored with a fiber optical thermo-sensor, which was placed 1 cm below the liquid surface. Two different blanks, PBS buffer solution (pH 7.4, 10 mM) and gold nanosphere suspension (*ca.* 30 nm in diameter, 100 mg/L), were taken for comparison (Fig.7 and Fig. S7†).

For the remotely NIR-triggered release behaviours, 1.5-mL of RB-loaded GNR@PEG-b-PNVCL in PBS buffer solution (150 mg/L, pH 7.4) was added in a Float-A-Lyzer G2 (*Spectra/Pro*®) dialysis device with the cap opened, and then dialyzed against 5 mL of PBS buffer solution (pH 7.4, 10 mM) inside a 37 °C water bath. The distance between the laser diode and the liquid surface

was also set at 0.5 cm. At each pre-determined interval upon NIR irradiation (802 nm, 100 or 150 mW), samples were withdrawn to determine the release amount spectrophotometrically via the above-mentioned protocol. Release profiles under different NIR powers were also presented in cumulative mode (Fig. 9a). Evolution of temperatures of the release medium upon the application or removal of NIR irradiation (Fig. 9b) was followed with a fibre optical thermo-sensor, which was also placed 1 cm below the liquid surface.

Cell culture and cytotoxicity assessment

The fibroblast-like L929 cell line was obtained from ATCC (*ATCC CCL-1*). L929 cells were grown at 37 °C under humidified air containing 5 *vol*.% of CO_2 in GIBCO Dulbecco's modified eagle medium (DMEM, 4.5 g/L of glucose) supplemented with 5 *vol*.% of fetal bovine serum (FBS, Gibco), 1 *vol*.% of glutamax, 1 *vol*.% of penicillin/streptomycin (10,000 units of penicillin and 10,000 units of streptomycin /mL) (DMEM complete medium). After 24-h incubation, the cells were rinsed with PBS (Ca^{2+}/Mg^{2+} free) buffer solution, and then detached with trypsin (0.2 *vol*. %)/PBS (Ca^{2+}/Mg^{2+} free) buffer solution.

The L929 cells were seeded in 96-well plates with a density of 5×10^3 cells/well and grown in DMEM complete medium for another 24 h. The cells were then treated with GNR@CTAB or GNR@PEG-*b*-PNVCL suspensions in DMEM complete medium with different concentrations (10, 50, 100 and 200 µg/mL). For each concentration, 5 parallel samples were repeated at the same time. After a pre-determined incubation period, the cells were rinsed with PBS buffer solution (with Ca^{2+}/Mg^{2+}), and cell viabilities were evaluated via the MTS assay. 20 µL of MTS in 100 µL of PBS buffer solution (with Ca^{2+}/Mg^{2+}) were added, and then the cells were incubated for 30 min at 37 °C. The absorbance at 490 nm was measured using a Power wave X (Biotek Instrument Inc.) micro-plate reader. Percentages of the cell viabilities were determined relative to the untreated cells taken as a control (100% viability).

Characterization

Dynamic light scattering (DLS) measurements were carried out with a Malvern Instrument Nano-ZS, equipped with a He-Ne laser ($\lambda = 663$ nm) and scattering angle of 90°. The correlation function was analyzed via the CONTIN method, and D_h was determined using the Stokes-Einstein equation. The averaged D_h was obtained from three different runs. Standard deviation was used to evaluate the size distribution (PDI). Electrophoresis mobility of the GNR@PEG-*b*-PNVCL or GNR@CTAB suspension was checked at 25 °C and zeta potential (ζ) was obtained via the Smoluchowski approximation. The mean value was obtained by averaging data from three independent runs.

Transmission electron microscopy (TEM) was used to measure the size and size distribution of the gold nanorods with a Philips CM-100 microscope. A drop of GNR@PEG-*b*-PNVCL aqueous suspension was placed onto a carbon-coated copper grid and left to dry in air. Then the samples were negatively stained with uranyl acetate (2 *wt*. %, 2 min). The size distribution was analyzed by sampling *ca*. 200 particles on the TEM images.

X-ray diffraction (XRD) pattern of the GNR@PEG-*b*-PNVCL was recorded by a Philips PW1700 diffractometer with Cu/Kα irradiation ($\lambda = 1.5418$ Å).

Thermogravimetric analysis (TGA) of the PEG-*b*-PNVCL copolymers or GNR@PEG-*b*-PNVCL after free-drying was performed by heating to 100 °C at 50 °C/min and equilibrating for 10 min, and then TGA curves were recorded upon heating to 600 °C at 20 °C/min in air with a TA Q100 Instrument.

^{1}H Nuclear magnetic resonance (NMR) spectra of the PEG or PEG-*b*-PNVCL macromolecules were recorded with a 250 MHz Bruker spectrometer in $CDCl_3$ at 25 °C and in D_2O at 25 or 50 °C.

Size-exclusion chromatography (SEC) was performed in THF (flow rate: 1 mL/min) at 40 °C using a Waters 600 liquid chromatograph equipped with a 410 refractive index detector and styragel HR columns (four columns HP PL gel 5 µm, 10^5 Å, 10^4 Å, 10^3 Å and 10^2 Å), calibrated with polystyrene standards.

Turbidity measurement of the PEG-*b*-PNVCL copolymers was carried out with a Hitachi U-3300 UV/*vis* spectrometer equipped with an external water bath. The polymer solution (0.1 *wt*. %) was heated at 1 °C/min from 25 to 60 °C, and transmittance at 700 nm was plotted against the temperature, while cloud point temperature (T_c) was taken from the temperature where transmittance started to decrease.

UV/vis spectra of the GNR@CTAB or GNR@PEG-*b*-PNVCL aqueous suspensions were recorded between 200 and 900 nm with a Hitachi U-3300 spectrophotometer. To study the thermo-dependent optical properties, UV/*vis* adsorption spectra were recorded with the GNR@PEG-*b*-PNVCL aqueous suspension (50 µg/mL) under different temperatures, with the help of the external water bath.

X-ray photoelectron spectroscopy (XPS) of the GNR@PEG-*b*-PNVCL after freeze-drying was recorded with a VG Scientific 220 i-XL ESCALAB spectrometer at 100 W (10 kV and 10 mA), which is equipped with a non-monochromatised MgKα source ($hv = 1253,6$ eV). A pressure of 10^{-7} Pa was maintained in the chamber during analysis. The analyzed area was *ca*. 150 µm in diameter. The full spectra (0-1150 eV) were obtained with constant pass energy of 150 eV and high-resolution spectra at constant pass energy of 40 eV. Charge neutralization was required for insulating samples. The peaks were referenced to C1s peak at 284.7 eV.

Fourier transform infrared spectra (FTIR) of the GNR@PEG-*b*-PNVCL or PEG-*b*-PNVCL copolymers after freeze-drying were recorded with a Perkin Elmer FTIR instrument. Samples were mixed and grinded with potassium bromide (KBr), and then compressed for characterization.

ICP/OES analysis of the GNRs aqueous suspension was carried out with an inductively coupled plasma optical emission spectrometry (ICP/OES 720ES Varian). 0.1 mL of the GNRs suspension was mixed with 1 mL of HCl/HNO₃ acid mixture (3/1 *vol*./*vol*.), in order to dissolve the GNRs. After neutralization with 2.0 M NaOH solution, the solution was diluted to 50 mL, and then used for elemental analysis via ICP measurement.

Results and discussion

Preparation of poly(ethylene glycol)-*b*-poly(*N*-vinylcaprolactam) (PEG-*b*-PNVCL) block copolymers

N-vinylcaprolactam (NVCL) is an unconjugated monomer that can only be polymerized radically.[47] Up to now, only few works have been reported on the living radical polymerization of NVCL using cobalt complexes[48, 49] and xanthates.[38, 50] In the first strategy named

"cobalt-mediated radical polymerization (CMRP)",[51-53] NVCL polymerization was controlled by Co(acac)$_2$, a commercially cheap reagent. Various block copolymers such as poly(vinyl acetate)-*b*-poly(*N*-vinylcaprolactam) (PVAc-*b*-PNVCL), poly(vinyl alcohol)-*b*-poly(*N*-vinylcaprolactam) (PVOH-*b*-PNVCL) copolymers,[48] and double thermo-responsive poly(*N*-vinylcaprolactam)-*co*-poly(*N*-methyl-*N*-vinylacetamide) (PNVCL-*co*-PNMVA) copolymers,[49] were made available via this technique. Additionally, "reversible addition-fragmentation transfer (RAFT)" polymerization was also reported to impart good control over the polymerization of NVCL;[38, 54] PNVCL homopolymer[38, 50, 54] and various copolymers, such as poly(vinyl acetate)-*b*-poly(*N*-vinylcaprolactam),[54] poly(ε-caprolactone)-*b*-poly(*N*-vinylcaprolactam),[55] and linear-dendritic (polyamide dendrons)-*b*-poly(*N*-vinylcaprolactam) diblock copolymers,[56] were synthesized. Moreover, as a well-established polymerization strategy, RAFT technique manifests itself with the presence of trithiocarbonate, dithioester, or xanthate end-groups, which further makes those RAFT-prepared polymers appealing for the preparation of gold hybrid organic-inorganic nanoparticles.[35] In this work, well-defined PEG-*b*-PNVCL copolymers with different PNVCL block lengths and end-capped by a xanthate group are synthesized via the RAFT technique. The main goal is to utilize these xanthate-end macromolecules to form a functional polymer corona over the gold nanorods (GNRs), which are further exploited as DDS for remotely triggered release.
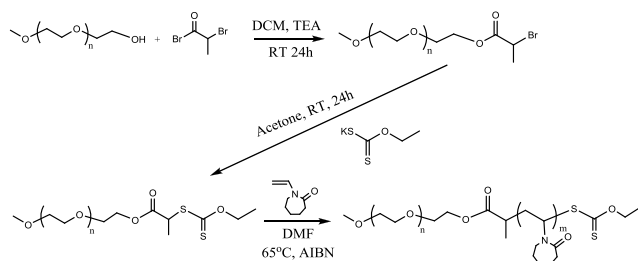
Scheme 1 Preparation of mPEG$_{114}$-X macro-CTA, and synthesis of PEG-*b*-PNVCL copolymers via RAFT polymerization in DMF at 65 °C

To polymerize NVCL monomers via RAFT polymerization, poly(ethylene glycol) methyl ether was first converted to mPEG$_{114}$-X macro-CTA via a two-step modification of the ω-chain end (Scheme 1). The first step involves the reaction of the hydroxyl end-group of mPEG$_{114}$-OH with 2-bromopropionyl bromide in the presence of triethylamine. Potassium ethyl xanthogenate is then reacted in a second step with this modified mPEG$_{114}$-Br to prepare the final mPEG$_{114}$-X macro-CTA.

Fig. S1a† shows the typical ^{1}H NMR spectrum of the resultant mPEG$_{114}$-Br obtained after the first-step modification. The incorporation of 2-bromopropionyl end-group is confirmed from the presence of methine (^{c}H) and methyl (^{e}H) protons at δ of 4.3 and 1.8 ppm, respectively (see ESI, Fig. S1a†). Similarly, in the second step, potassium ethyl xanthogenate is introduced via the elimination reaction of KBr. The resultant mPEG$_{114}$-X macro-CTA is confirmed with the new peaks at δ of 4.3 and 1.6 ppm, assignable to the methylene (^{g}H) and methyl (^{h}H) protons in the xanthogenate end-group (see ESI, Fig. S1a†). The observed M_n from SEC analysis in THF are 8300 and 8500 g/mol (eq. PS) for the

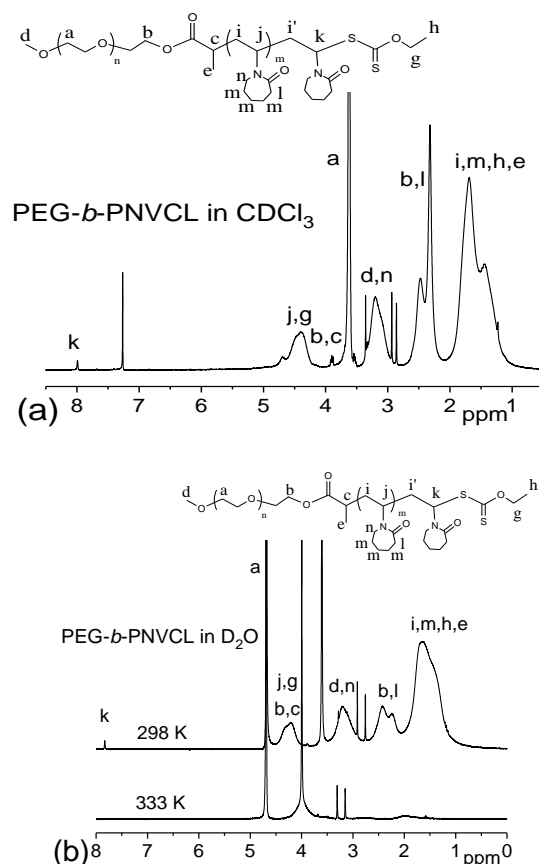mPEG$_{114}$-Br and mPEG$_{114}$-X, respectively (see ESI, Fig. S1b†), with no change in PDI (1.02).

Fig. 1 Representative ^{1}H NMR spectra of PEG$_{114}$-*b*-PNVCL$_{59}$ copolymer in CDCl$_3$ at 25 °C (a), ^{1}H NMR spectra in D$_2$O at 25 °C and 50 °C (b).

The as-prepared mPEG$_{114}$-X macro-CTA is then used to control the radical polymerization of NVCL at 65 °C in DMF (Scheme 1). Typical ^{1}H NMR spectrum of the PEG-*b*-PNVCL copolymers is shown in Fig. 1. In addition to the characteristic signals from PEG$_{114}$-X macro-CTA in Fig. S1a†, new peaks originating from PNVCL block are also observed in ^{1}H NMR spectra of PEG-*b*-PNVCL copolymers in Fig. 1a (in CDCl$_3$) and Fig. 1b (in D$_2$O), with all the peaks marked. Table 1 also summarizes all the parameters of PEG-b-PNVCL copolymers prepared from different feeding ratios ([M]$_0$/[I]/[CTA]), with monomer conversion in the range of 30-40%. As expected, the observed molecular weight ($M_{n, SEC}$) obtained from SEC analysis in THF increases with higher feeding ratio of [M]$_0$/[I], and the molecular weights ($M_{n,cal}$) calculated on the basis of monomer conversion are close to the molecular weights ($M_{n,NMR}$) estimated from ^{1}H NMR analysis. Unimodal SEC chromatograms are observed for each PEG-*b*-PNVCL copolymer with PDI no higher than 1.06. The observed difference in $M_{n,NMR}$ and $M_{n,SEC}$ is due to the use of polystyrene as standards for the SEC calibration.

In order to evaluate the livingness of the polymerization of NVCL using mPEG$_{114}$-X as macro-RAFT agent, studies on polymerization kinetics are carried out with the polymerization in DMF at 65 °C with a feeding ratio [M$_0$]/[I]/[CTA] of 200/0.2/1, as

listed in Table 1 entry 2, and the kinetics is monitored with ^{1}H NMR (CDCl$_3$) and SEC (THF) analysis. Fig. 2a shows the plotting of ln([M$_0$]/[M]) against polymerization period, and it increases almost linearly up to 35% conversion, however, did not follow a first order reaction kinetic. Fig. 2b shows the dependence of M_n and M_w/M_n on monomer conversion (%). $M_{n,SEC}$ increases linearly, indicating that all the chains are growing during the entire polymerization procedure. The observed deviation of $M_{n,SEC}$ from $M_{n,cal}$ is also due to the use of polystyrene standards in SEC analysis. SEC chromatograms exhibit a shift to lower elution time and thus higher molecular weights with the increase of monomer conversion (Fig. 2c). Furthermore, narrow molecular weight distribution with M_w/M_n in the range of 1.02-1.04 is detected.
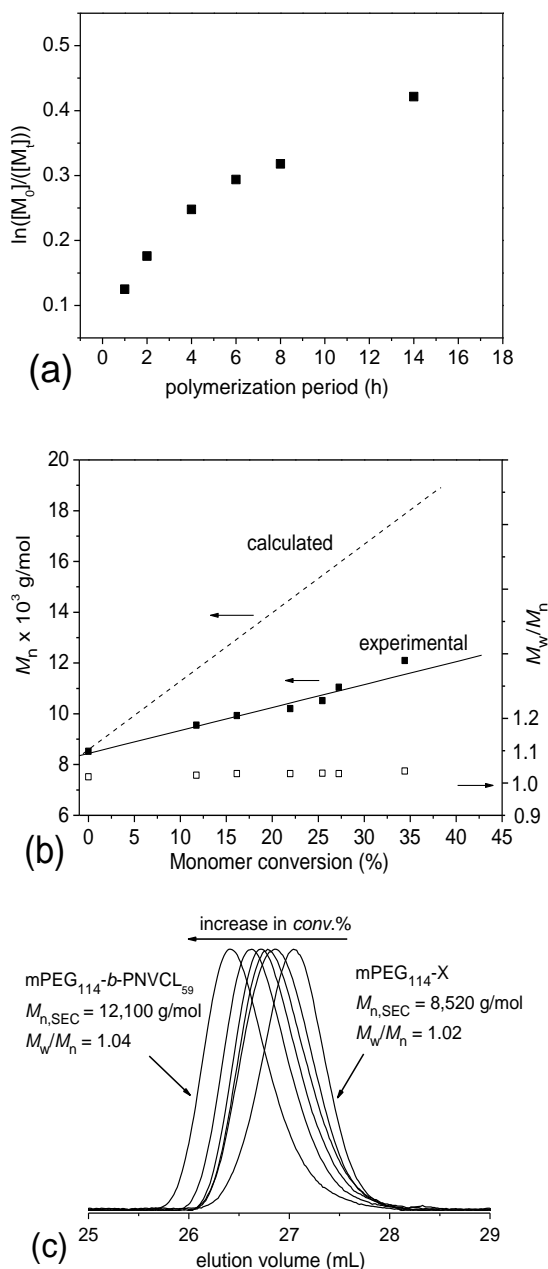
(a)

(b)

(c)

Fig. 2. Semi-logarithmic kinetics plotting of ln([M$_0$]/[M$_t$]) against polymerization period (a), dependence of theoretical and experimental M_n as well as M_w/M_n (PDI) on monomer conversion (b), and SEC traces of PEG-b-PNVCL copolymers from different monomer conversions (c) for the polymerization of NVCL with mPEG$_{114}$-X macro-CTA at 65 °C in DMF. Polymerization conditions: [M$_0$]/[I]/[CTA] = 200/0.2/1 mol. and [NVCL]/[DMF] = 1/3 wt./vol.%. The theoretical molecular weight $M_{n,cal}$ in (b) is represented by the dotted line and calculated according to the [M$_0$]/[CTA] feeding ratio and monomer conversion determined via ^{1}H NMR analysis in CDCl$_3$, and the experimental molecular weight $M_{n,SEC}$ is represented by the solid line and obtained from SEC analysis in THF with polystyrene as the calibration standard.

Thermo-responsiveness of the PEG-b-PNVCL block copolymers

Similar to PVOH-b-PNVCL[48, 57] and PNVCL-co-PNMVA[49] copolymers in our previous works, the as-prepared PEG-b-PNVCL copolymers are also expected to undergo a thermo-induced phase transition due to the hydrophobic essence of PNVCL block above its T_c. ^{1}H NMR spectroscopy is first used to investigate the thermo-responsiveness of the PEG-b-PNVCL copolymers in aqueous solution. Fig. 1b shows the temperature-dependent ^{1}H NMR spectra for PEG$_{114}$-b-PNVCL$_{59}$ (0.1 wt. %) in D$_2$O. At 25 °C, the block copolymer is expected to be dissolved as unimers below its LSCT of 46 °C obtained from turbidimetric analysis (discussed in details later). Thus characteristic peaks arising from both PEG and PNVCL blocks are readily visible. However, the increase of the temperature to 50 °C leads to the dehydration and collapse of the hydrophobic PNVCL block, as evidenced by the attenuation of peaks associated with PNVCL block, while the PEG peaks are still present.

Turbidimetric measurements are also carried out to investigate the thermo-responsiveness and thermal-induced phase transition of the PEG-b-PNVCL aqueous solutions (1 g/L) under gradual heating (Fig. 3a). For PEG-b-PNVCL with longer PNVCL block length (PEG$_{114}$-b-PNVCL$_{59-237}$), the aqueous solutions are very sensitive to a transmittance change within a narrow temperature range. While for that with shorter block length, e.g. PEG$_{114}$-b-PNVCL$_{24}$, the transmission could not decrease to zero, similar to the finding of Aoyagi[58], due to the relative short block length of thermo-responsive segment. It is observed that T_c is closely depended on the PNVCL block length. As reported previously, T_c is usually decided by a lot of factors, such as molecular weight (block length), molecular weight distribution, chemical composition, nature of the co-monomer, polymer concentration, heating rate.[58]

increase in conv.%

mPEG$_{114}$-b-PNVCL$_{59}$
$M_{n,SEC}$ = 12,100 g/mol
M_w/M_n = 1.04

mPEG$_{114}$-X
$M_{n,SEC}$ = 8,520 g/mol
M_w/M_n = 1.02

Tab. 1 Parameters of the PEG-b-PNVCL copolymers

Structure [a]	Feeding ratios [M$_0$]/[I]/[CTA]	$M_{n\,cal}$ [b] g/mol	$M_{n,NMR}$ [c] g/mol	$M_{n,SEC}$ g/mol	M_w/M_n	Reaction time h	Conv. [d] %	T_c [e] °C
PEG$_{114}$-b-PNVCL$_{24}$	50/0.2/1	7,700	8,500	9,800	1.04	17	39	49
PEG114-b-PNVCL$_{59}$	200/0.2/1	14,600	13,200	12,100	1.04	14	34	46
PEG$_{114}$-b-PNVCL$_{125}$	450/0.2/1	24,800	22,400	14,400	1.03	14	32	41
PEG$_{114}$-b-PNVCL$_{237}$	800/0.2/1	41,200	38,000	15,000	1.06	16	33	39

Polymerization conditions: [NVCL]/[DMF] = 1/3 $wt./vol.$%, reaction temperature of 65 °C.
[a] block length of PNVCL is calculated from the molar ratio between the PEG and PNVCL block from the ^{1}H NMR analysis in CDCl$_3$
[b] calculated from $M_{n, cal} = M_{mPEG} + conv.$% * [M]$_0$/[CTA]*(molar mass of NVCL)
[c] calculated from $M_{n, NMR} = M_{mPEG} + M_{PNVCL}$, M_{PNVCL} was estimated from molar ratio between the PEG and PNVCL block via ^{1}H NMR analysis in CDCl$_3$
[d] monomer conversion determined by ^{1}H NMR analysis in CDCl$_3$
[e] T_c determined from the turbidimetric measurement (0.1 $wt.$%), heating rate of 1 °C/min, and T_c was taken at the temperature where transmittance started to decrease
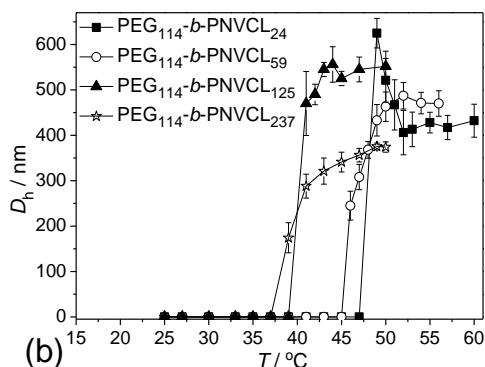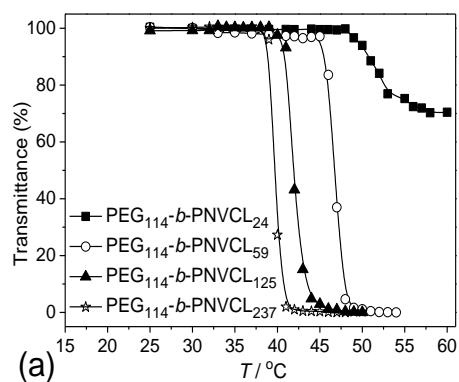

Fig. 3 Plotting of transmission *vs.* temperature for the PEG-b-PNVCL copolymer aqueous solutions (1 g/L) with different PNVCL block lengths under gradual heating (1 °C/min) via turbidimetric measurements, T_c was taken at the temperature where transmittance started to decrease (a); and dependence of D_h on temperature for the PEG-b-PNVCL copolymer solutions (1 g/L) with different PNVCL block lengths via DLS analysis (b). The solid lines here just serve to guide the eyes.

For those narrow-dispersed PNVCL homopolymers,[38] decrease in M_n is in favour of higher T_c. When thermo-responsive block copolymers are considered, T_c would be also affected by the nature

of co-monomers and each block length. Here, with a fixed length of the hydrophilic PEG$_{114}$ block, the decrease in the block length of PNVCL also results in the increase of T_c (Tab. 1 and Fig. 3a). Therefore, T_c of the PEG-b-PNVCL copolymers could be tuned to few degrees above the physiological temperature (37 °C), aiming for some specific biomedical applications, such as thermo-triggered drug release.

DLS is another versatile technique to study the thermo-responsiveness by monitoring the thermo-induced self-assembly of polymer micelles. In Fig. 3b, D_h of the PEG-b-PNVCL aqueous solutions (1 g/L) under different temperatures is plotted against T, and a dramatic increase in D_h within a very narrow temperature range is detected, despite of their polymer compositions. This is attributed to the thermo-induced dehydration of the PNVCL block above its T_c, thus thermo-induced physically-assembled micelles might be generated. Similar to our previous PVOH-b-PNVCL system,[48, 57] when the temperature is further increased, the hydrophilicity of PNVCL cores becomes worse and worse, and inter-micelles collapse might occur to form larger aggregates, in order to reduce the total surface energy. Phase change temperature (where the formation of micelles occurred), is observed near the T_c, and it also increases with the decrease of PNVCL block length.

Preparation of thermo-responsive GNR@PEG-b-PNVCL nanoparticles

The seed-mediated approach to prepare GNRs has been well-documented.[14] It consists of the reduction of gold salts with a strong reducing agent (NaBH$_4$) to obtain gold seeds. The afterward controlled growth of GNRs from the former gold seeds is then carried out in the presence of CTAB as surface-directing agents. In this study, the seed-mediated growth protocol is also used to prepare GNRs, with the averaged size of *ca.* 18 ± 4 nm in width and 69 ± 8 nm in length from TEM observation (see ESI, Fig. S2†), *i.e.* estimated aspect ratio of *ca.* 3.8.

After the synthesis and purification, the GNRs are further coated with RAFT-generated PEG-b-PNVCL copolymers, as shown in Scheme 2. Commonly, the RAFT-generated polymers can be immobilized onto the gold surface through the "grafting to" approach via two different methods. The first one involves the mixing of the RAFT-generated polymers and gold nanoparticles in

a good solvent of the polymer, in the presence of a reducing agent, for example, NaBH$_4$, which reduces the ω-chain end of the polymer (xanthate in this case) into thiols.[35,36] The second technique is essentially the same, however, without the reducing agent. Recently some reports have demonstrated the possibility of immobilizing dithioester- or trithiocarbonate-ended polymers on the gold surfaces via the preferential Au-S bonding without reductive agent.[37-41, 59, 60]
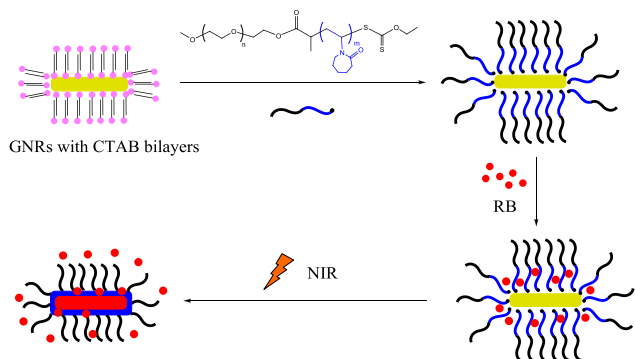
Scheme 2 Preparation of GNR@PEG-*b*-PNVCL, guest loading of Rhodamine® B (RB) and remotely triggered release of RB by near infrared (NIR) activation

Here, immobilization of the xanthate-ended PEG-*b*-PNVCL copolymers onto gold nanorods is also carried out by mixing GNRs and PEG$_{114}$-*b*-PNVCL$_{237}$ copolymer (T_c of 39 °C) in aqueous medium without the reductive agent. Excess of unbound copolymers are eliminated via centrifugation. TEM image of GNR@PEG-*b*-PNVCL is shown in Fig. 4a, in which the polymer shell is clearly observed after negative staining, compared with the TEM image of the GNRs before coating in Fig. S2†. The polymer fraction is estimated to be *ca*. 12 *wt*. % via thermogravimetric analysis (TGA, Fig. 4b). Based on this value, the surface grafting density is estimated to be *ca*. 0.2 chain/nm^2, comparable to the value of *ca*. 0.75-1.04 chain/nm^2 reported by Toth[41] on coating of gold nanospheres (5-17 nm) with RAFT-polymerized PNIPAM$_{43}$. Since increase in the chain length leads to an increase in the steric hindrance of ligands, and thus to the decrease of grafting density, the lower grafting value obtained for our copolymer is reasonable. Similar to other polymer-coated gold nanoparticles,[38-40] a slight red-shift (*ca*. 10 nm) in both transverse and longitudinal SPR band upon polymer coating is also observed (see ESI, Fig. S4a†), due to the changes in local dielectric coefficient and surface refractive index. It also deserves to be mentioned that there is no broadening of the SPR peak, which indicates the absence of GNRs aggregation upon coating with PEG-*b*-PNVCL. A large increase in hydrodynamic diameter for GNR@PEG$_{114}$-*b*-PNVCL$_{237}$ (D_h of 280 nm) compared to initial GNRs (D_h of 60 nm) is confirmed with the size distribution pattern (see ESI, Fig. S4b†) and correlograms (see ESI, Fig. S4c†) from DLS analysis. The difference between sizes from DLS and TEM analysis results from the hydrated and swelling state of the polymer corona for the DLS samples, while dehydrated and dense polymer shell for the latter. Mobility measurement clearly corroborates a neutral surface (ζ of *ca*. -5.1 mV at pH 7.4) for GNR@PEG$_{114}$-*b*-PNVCL$_{237}$ after polymer coating, compared with the formerly positively-charged surface (ζ of *ca*. +36.5 mV at pH 7.4) with CTAB surfactants.

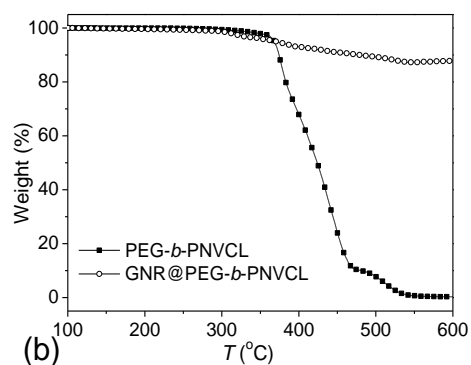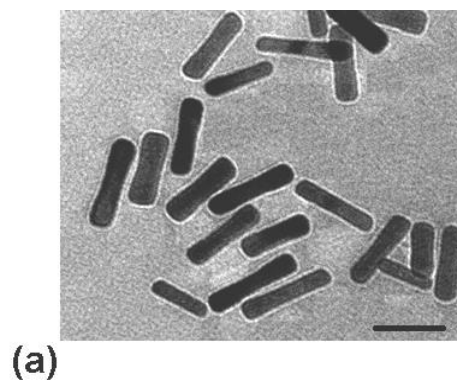**Fig. 4** Representative TEM image (a, scale bar: 50 nm) and TGA trace (b) of the GNR@PEG$_{114}$-*b*-PNVCL$_{237}$.

The presence of GNRs cores is also confirmed by XRD pattern (see ESI, Fig. S5a†) with the diffraction peaks arising at 44.2, 64.7 and 77.2, attributed to the (200), (220) and (311) crystal planes of the gold face cantered cubic (fcc) lattices.[61] XPS spectrum (see ESI, Fig. S5b†) of the GNR@PEG$_{114}$-*b*-PNVCL$_{237}$ also favourably corroborates the presence of PEG-*b*-PNVCL coating. Representative FTIR spectrum of the PEG$_{114}$-*b*-PNVCL$_{237}$ and the GNR@PEG$_{114}$-*b*-PNVCL$_{237}$ are illustrated in Fig. S5c†. Characteristic peaks from PEG-*b*-PNVCL copolymers at 1700 and 3100 cm^{-1} are attributed to the $v_{C=O, s}$ and $v_{O-H, s}$ vibrations, which are also observed in the spectrum of the as-prepared GNR@PEG-*b*-PNVCL. Moreover, good dispersion of the resultant GNR@PEG$_{114}$-*b*-PNVCL$_{237}$ in de-ionized water, THF, CH$_2$Cl$_2$ and DMSO was also confirmed (see ESI, Fig. S5d†), in agreement with the external PEG corona.

Thermo-responsiveness and thermo-dependent optical properties of the GNR@PEG-*b*-PNVCL nanoparticles

Due to the thermo-responsive essence of the PEG-*b*-PNVCL copolymers, GNR@PEG-*b*-PNVCL nanoparticles are also expected to retain this property. DLS is first used to follow the change of D_h as well as size polydispersity (PDI) of the GNR@PEG$_{114}$-*b*-PNVCL$_{237}$ aqueous suspension (50 μg/mL) upon heating (Fig. 5, solid). At 25 °C, the PEG-*b*-PNVCL polymer chain is hydrophilic and forms a solvated polymer corona over the GNRs, resulting in a large D_h of *ca*. 280 nm (PDI 0.25). Slight change is observed in D_h below 38 °C (T_c of 39 °C for PEG$_{114}$-*b*-

PNVCL$_{237}$). Upon heating, D_h decreases sharply afterward, and then levels off above 44 °C (180 nm and PDI 0.13 at 50 °C). The decrease in D_h can be easily explained by the dehydration of PNVCL block above its T_c, resulting in a compact polymer corona. The evolution of D_h and PDI upon cooling is also followed (Fig. 5 open), and similar size was detected with the heating run at the same temperature. The results corroborate the reversibility of the thermo-responsiveness. For those previously-reported gold nanoparticles coated with thermo-responsive homopolymer, such as GNP@PNVCL,[38] GNP@PNiPAAm[44] and GNR@PNiPAAm,[42, 45] thermo-induced agglomeration occurred with sharp increase in size and size distribution (PDI) above the T_c. Furthermore, most of them exhibited a T_c below physiological temperature (37 °C); therefore, further biomedical application was limited for these systems. In the case of PEG-b-PNVCL copolymers, T_c could be tuned to be few degrees above the physiological temperature by introducing PEG block and controlling the PNVCL block length, for example, 39 °C for PEG$_{114}$-b-PNVCL$_{237}$. Thus a good dispersion of the GNR@PEG$_{114}$-b-PNVCL$_{237}$ is detected under physiological condition. In addition, due to the steric repulsion role originating from PEG blocks, stable dispersion could also be obtained above the T_c, evidenced by the absence of size increase and PDI increase in Fig. 5 (> 39 °C). The observed large difference in D_h, as well as hydrodynamic volume (V_h) between above and below the T_c, is then envisaged to trigger the release of a pre-loaded drug upon shrinkage of the polymer corona.
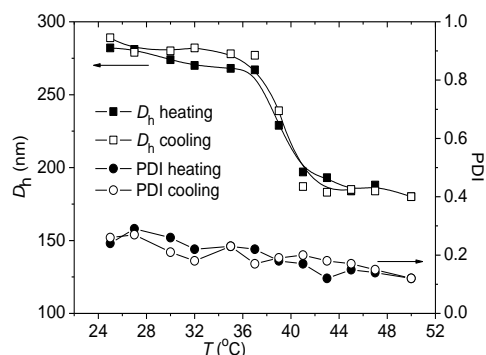
Fig. 5 Evolution of D_h and PDI of the GNR@PEG$_{114}$-b-PNVCL$_{237}$ aqueous suspension (50 μg/mL) upon heating (solid) and cooling (open). The solid lines here just serve to guide the eyes.

A thermo-induced red-shift has even been reported with thermo-responsive GNPs, such as GNR@PNiPAAm,[42, 45] GNP@PNiPAAm,[40, 42, 44] and GNP@PNVCL[38]. Here, thermo-dependent optical properties of the GNR@PEG$_{114}$-b-PNVCL$_{237}$ aqueous solution (50 μg/mL) are also investigated under different temperatures with a UV/vis spectrometer, equipped with an external water bath to tune the measurement temperatures. Fig. 6a shows the UV/vis absorbance spectra from 25 °C (solvated and swelling polymer corona) to 50 °C (collapsed and compact polymer corona). As expected, the longitudinal SPR band remains at nearly the same wave length below 40 °C; however, $ca.$ 28-nm red-shift of the SPR band is observed afterward. Usually the red-

shift is induced by the thermo-induced collapse of polymer corona or the inter-particles agglomeration, or both. In those previous reports on GNR@PNiPAAM[42,45] and GNP@PNiPAAm[44], the inter-particles agglomeration of the hydrophobic GNPs above the T_c was always accompanied with a broadened SPR band. Here, very slight SPR band broadening, if there is, is observed despite of the temperature above or below the T_c. Thus, this 28-nm red-shift of the SPR band above T_c is indeed caused by the thermo-induced collapse of polymer corona.
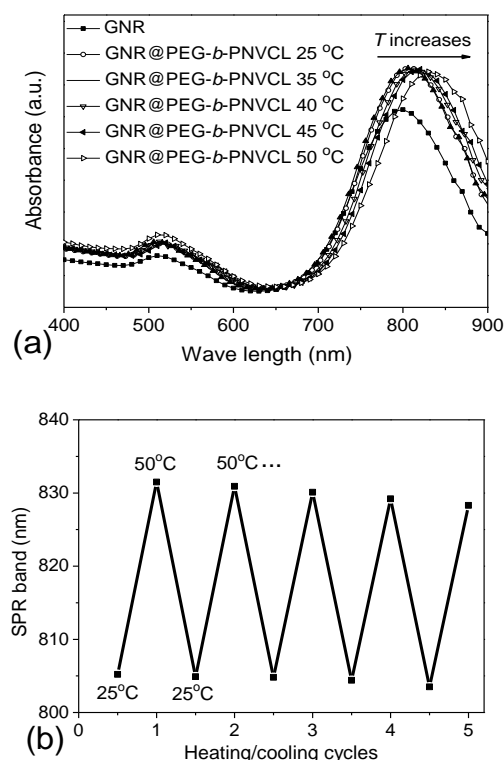

Fig. 6 UV/vis adsorption spectra of the GNR@PEG$_{114}$-b-PNVCL$_{237}$ aqueous suspension (50 μg/mL) under different temperatures (a); and evolution of longitudinal SPR band of the GNR@PEG$_{114}$-b-PNVCL$_{237}$ aqueous suspension (50 μg/mL) during multiple cooling (25 °C)/heating (50 °C) cycles (b). The solid lines here just serve to guide the eyes.

Furthermore, this also corroborated superior stability of the GNR@PEG-b-PNVCL above the T_c, due to the presence of the PEG blocks, in agreement with the results from DLS analysis in Fig. 5. Because of the reversible thermo-responsiveness as revealed by DLS analysis in Fig. 5, the thermo-induced shift of SPR band is also expected to be fully reversible. In Fig. 6b, the reversibility is evaluated by multiple cooling (25 °C)/heating (50 °C) cycles, and good reproductive shifts in SPR band are observed. It is deserved to be noted that, a very slight decrease of SPR band could be detected during the alternative heating/cooling treatment, and this might be attributed to the shape transformation of the GNR from larger aspect ratio to lower one, and/or detachment of the polymer coating. In our previous work on GNR@poly(caprolactone)-b-poly(ethylene glycol),[32] the GNR could tolerate 50 °C-heating for at least 30 min with nearly no

change in SPR band. On the other hand, we recorded a new TGA trace of the GNR@PEG-*b*-PNVCL sample after five-cycle heating/cooling treatment, a very slight difference in polymer fraction (*ca.* 0.85 *wt.*%) was detected, which might contribute to the shift of SPR band in Figure 6b. Anyway, this kind of thermo-dependent optical properties of the as-prepared GNR@PEG-*b*-PNVCL and its excellent reversibility might also be of interest for the design of biosensors that are sensitive to a certain local overheating.

Local heating induced by NIR laser irradiation

Gold nanorods have been explored as localized heating mediators due to their tunable SPR band via control over the aspect ratio, low-level of photoemission quantum yield[62] and large extinction coefficient at the SPR band, for example, 4.6×10^9 M^{-1} cm^{-1} at *ca.* 800 nm for GNRs with aspect ratio of *ca.* 4.0 reported by Murphy.[63] Generally, the heating mechanism involves the energy absorbed upon plasmon excitation, and the afterward energy re-emitting via non-radiative pathways, resulting in heating of the surroundings.[1] As a new class of external stimuli, NIR light (650-900 nm) exhibits a maximal penetration into the tissues due to the minimal optical absorption by physiological components such as hemoglobin (< 650 nm) and water (> 900 nm), thus biomedical treatment under NIR irradiation could be accomplished without significant side effects.[13] Up to now, this NIR-induced local heating was explored for remotely-triggered release,[25-34] tumour treatment via photothermia[15-24] and photoacoustic imaging.[24] In this study, with a PEG-*b*-PNVCL thermo-responsive corona, the internal heating generated by the GNRs upon NIR irradiation could lead to thermo-induced phase transition of PNVCL block, followed with a sharp collapse of the polymer corona, resulting in squeezing out of the majority of those water and pre-loaded drug molecules. Thus, remotely NIR-triggered drug release could be envisaged for the as-prepared GNR@PEG-*b*-PNVCL.

To justify this, heating efficiency of the GNR@PEG-*b*-PNVCL is evaluated by exposing the GNR@PEG-*b*-PNVCL to NIR irradiation. In particular, GNR@PEG$_{114}$-*b*-PNVCL$_{237}$ suspensions in PBS buffer (pH 7.4) with a known concentration (75, 150 or 300 mg/L) is irradiated with a NIR laser diode, and a wave length of 802 nm is used because it matches the longitudinal SPR band of 805 nm for the GNR@PEG$_{114}$-*b*-PNVCL$_{237}$. Variation in temperature is followed with an optical thermo-sensor. As shown in Fig. 7a (200 mW, 802 nm) and Fig. S7a† (100 mW, 802 nm), temperature of the GNR@PEG$_{114}$-*b*-PNVCL$_{237}$ aqueous suspension steadily increases within the testing period. After 10-min 200-mW NIR irradiation, a heating-up of *ca.* 19 °C is measured for the GNR@PEG$_{114}$-*b*-PNVCL$_{237}$ aqueous suspension (300 mg/L) under NIR irradiation (200 mW, Fig. 7a). Importantly, a NIR-induced heating-up of less than 2 °C is observed for the PBS buffer solution without GNR@PEG$_{114}$-*b*-PNVCL$_{237}$ (blank). Gold nanospheres suspension in PBS buffer (100 mg/L, 30-nm diameter with SPR band at 520 nm) is also taken for comparison, and similar heating-up profiles as for the PBS blank is also observed in Fig. 7a. Moreover, the dependence of NIR heating profiles on irradiation power is also explored by testing five different laser powers: 50, 100, 150, 200 and 250 mW (Fig. 7b for GNR@PEG$_{114}$-*b*-PNVCL$_{237}$ and Fig. S7b† for PBS buffer

solution). Highly power-dependent heating-up behaviours are confirmed for the GNR@PEG-*b*-PNVCL aqueous suspension and PBS buffer solutions; however, slight heating up of the PBS buffer solutions is still observed despite of the irradiation powers. These results all evidence concentration- and irradiation power-dependent NIR-induced heating behaviours, as well as the dependence of heating capacity on the morphology of gold nanoparticles.
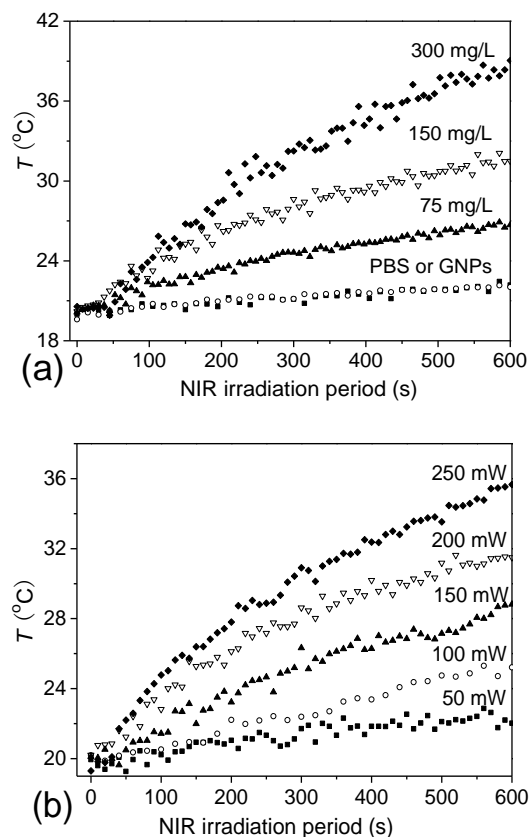

Fig. 7 Evolution of temperature of the GNR@PEG$_{114}$-*b*-PNVCL$_{237}$ aqueous suspensions with different concentrations upon NIR laser irradiation (200 mW, 802 nm) within 10 min (a), and evolution of temperature of the GNR@PEG$_{114}$-*b*-PNVCL$_{237}$ aqueous solution (150 mg/L) upon the NIR laser irradiation (802 nm) with different power outputs within 10 min (b); PBS buffer solution (pH 7.4, 10 mM) was taken as a blank, while another blank of gold nanospheres aqueous suspension (GNP, *ca.* 30 nm in diameter, SPR band of 520 nm, 100 mg/L) was also taken for comparison, to evidence the dependence of heating capacity of gold nanoparticles on their morphology.

As discussed previously, tumour cells are known to be sensitive to slight temperature increase during the magnetic hyperthermia treatment,[12, 64, 65] which is also critical to the success of clinical tumours treatment via NIR-induced photothermia. Tumour cells apoptosis happens above 42 °C, due to the protein denaturation caused by overheating, whereas normal cells could still survive for a specific period.[12] As showed in the NIR-heating experiments, the local heating as well as heating of the surrounding medium are highly dependent on the GNRs concentration,

irradiation power and period. Thus, it is plausible to anticipate that through further optimizing the GNR@PEG-*b*-PNVCL with targeting moieties, coupling with the control over NIR laser powers, an optimal local heating could be achieved, which is not
5 harmful to the healthy tissues, but high enough to cause apoptosis of most tumour cells. Furthermore, it could also be exploited to NIR-triggered drug release, taking advantage of the thermo-responsive polymer corona, as it will be discussed later.

10 **Model studies on guest loading capacity and triggered release behaviours of the GNR@PEG-*b*-PNVCL as DDS**

To test the capability of drug loading and triggered release of the as-prepared GNR@PEG-*b*-PNVCL as DDS, Rhodamine® B (RB), a hydrophilic model drug, is loaded into the polymer corona.
15 The presence of RB in the RB-loaded GNR@PEG-*b*-PNVCL aqueous suspension is confirmed in its UV/*vis* spectrum in Fig. 8a. Drug loading capacity (*DLC*) of *ca*. 2.2 *wt*. % and drug loading efficiency (*DLE*) of *ca*. 27.5% are determined spectrophotometrically. This relative low loading capacity is
20 relative to the low polymer fraction and also the weak van der Waals' interaction between the RB molecules and PEG-b-PNVCL polymer chains. Similar to those thermo-responsive inorganic/organic DDS, such as Fe_3O_4@PNiPAAm,[66] Fe_3O_4@[poly(lysine)-*b*-(poly(ethylene oxide)-poly (propylene
25 oxide)-poly (ethylene oxide))],[67] γ-Fe_2O_3@poly(acrylic acid)-b-poly(vinyl alcohol),[68] *etc*, a temperature-dependent release behaviour is also detected here (Fig. 8b), due to the synergetic contribution of the thermo-induced collapsing of the polymer corona above the T_c and the enhanced diffusion coefficient at
30 higher temperatures. Due to the T_c of 39 °C for PEG_{114}-*b*-$PNVCL_{237}$ copolymer, a relative slow release is observed under physiological condition (37 °C), while higher temperature above the T_c results in an accelerated release, which is also expected to be achieved by NIR-irradiation, as explored in the former section.
35 As an especially attractive stimulus, light can be remotely applied with extremely high spatial precision, in order to trigger the drug release. Moreover, a broad range of parameters (wave length, power output and duration of exposure) can be adjusted to modulate the release profiles.[1] Recently, NIR irradiation, which
40 presents high penetration depth and minimal tissue damage, has been attempted for remotely-triggered drug release.[25-34] Here, due to the location of longitudinal SPR band in the NIR range, coupling with the NIR-induced heating capability as explored in the former section, possibility of remotely NIR-triggered release behaviours
45 of the RB-loaded GNR@PEG-b-PNVCL are also tested. Fig. 9a summarizes the NIR-triggered release profiles under multiple NIR laser on/off cycles with different laser powers, and cumulative release continuously increases with more laser on/off cycles. Faster release is detected during the NIR irradiation, whereas
50 release decreases after the removal of NIR irradiation, and power-dependent release behaviour is also observed. On the other side, evolution of temperatures of the release system is also followed and summarized in Fig. 9b. Similarly to the results in Fig. 7 and Fig. S7†, a sharp temperature increase is also observed in the first
55 10 min, and then levelled-off afterward. Importantly, the temperature drops down quickly to 37 °C promptly upon the removal of NIR irradiation. Higher heating-up of the release medium is detected under higher-power irradiation, similar to the

heating profiles in Fig. 7b. The deviation on heating-up between
60 Fig. 7 and Fig. 9b can be explained by the dilution effect of the release medium, similar to our previous finding when dealing with the magnetically-triggered drug release, with DDS based on maghemite cores and poly(vinyl alcohol)-*b*-poly(acrylic acid) corona.[68]
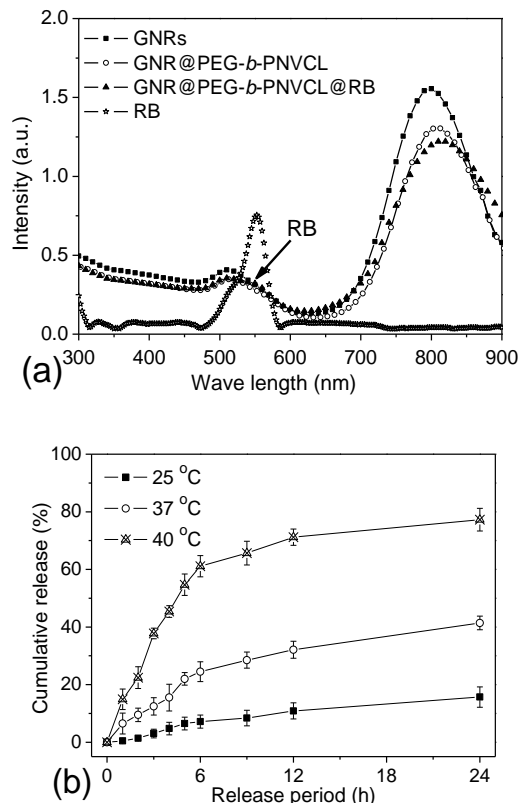
65

(a)

(b)

Fig. 8 UV/*vis* spectra of bare RB aqueous solution
(30 μM), GNRs (50 mg/L), GNR@PEG_{114}-*b*-
70 $PNVCL_{237}$, (50 mg/L) and RB-uploaded GNR@PEG_{114}-*b*-$PNVCL_{237}$ aqueous suspensions (50 mg/L) (a), and release profiles of RB from the RB-uploaded GNR@PEG_{114}-*b*-$PNVCL_{237}$ aqueous suspension (150 μg/mL) under different
75 temperatures (b). The solid lines here just serve to guide the eyes.

Compared with the release under conventional thermal heating, the NIR irradiation triggers the release much faster, even with almost the same heating-up of the release medium. For example,
80 under 100-mW NIR irradiation, the release medium is heated to *ca*. 39.5 °C, however, the release is much faster than that under 40 °C conventional heating (all above the T_c of 39 °C). This is most likely due to the fact that the laser excitation only heats an area of only few nm around the GNRs, and then the heat generated is
85 conducted across the polymer corona to the overall release medium. Therefore, we assume that the local temperature of the polymer corona is much higher than that of the overall medium, explaining why a faster release is observed under NIR irradiation. Similarly to the magnetically-induced heating,[12] the NIR-
90 irradiation might also be doubted on the risk of organs damage due to the local overheating. Here, given a fixed GNR@PEG-*b*-PNVCL concentration (150 μg/mL), a power-dependent heating-

up of the release medium is observed, for exactly, *ca.* 2.5 °C for 100 mW and *ca.* 5 °C under 150 mW. Therefore, further optimization could also be done by tuning the concentration of GNR@PEG-*b*-PNVCL and/or irradiation power in order to achieve a temperature where the release profile is obviously accelerated, while heating to the surrounding medium is minimal, for example the NIR-triggered release under 100 mW-irradiation.
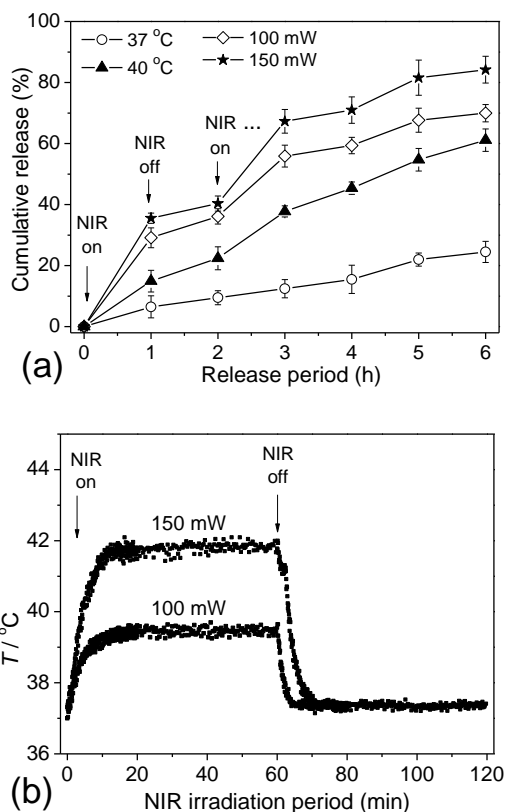

(a)

(b)

Fig. 9 Release profiles of RB-loaded GNR@PEG$_{114}$-*b*-PNVCL$_{237}$ aqueous suspension (150 mg/L) under NIR irradiation (802 nm) with different powers (100 and 150 mW), the marked arrows referred the application (NIR on) or removal (NIR off) of NIR irradiation, while 6-h release profiles at 37 and 40 °C as references were taken from parts of Fig. 8b (a); and evolution of temperatures of RB-loaded GNR@PEG$_{114}$-*b*-PNVCL$_{237}$ aqueous suspension (150 μg/mL) under NIR irradiation (802 nm) with different powers (100 and 150 mW) (b). The solid lines here just serve to guide the eyes.

Cytotoxicity of GNR@PEG-*b*-PNVCL against fibroblast-like L929 cell line

Cytotoxicity assessment is of necessity for those nanomaterials aimed for biomedical applications. Here, cytotoxicity potential of the GNR@PEG-*b*-PNVCL against mouse fibroblast L929 cell line is evaluated via the MTS assays. Cell viabilities of the L929 cells after maximal 72-h exposure to the GNRs with CTAB surfactants (Fig. 10a) and GNR@PEG$_{114}$-*b*-PNVCL$_{237}$ (Fig. 10b) with different concentrations are summarized. As shown in Fig. 10a, the cell proliferation is highly inhibited with GNRs without polymer coating, especially for those at higher concentrations comparing with the control. And even at the low dose of 10 μg/mL, only *ca.* 20% of the cells population are still viable after 72-h incubation, suggesting strong cytotoxicity of the GNR@CTAB. Similarly to the cytotoxicity profiles of CTAB alone and GNR@CTAB system reported in other previous literatures,[69, 70] CTAB molecules here are also responsible for the toxicity of GNRs prepared via the seed-mediated growth mechanism. This observation evidences the necessity to coat these GNRs with biocompatible ligands when biomedical applications are targeted. The MTS assay is also carried out to confirm the decrease in cytotoxicity potential of the GNRs after coating with PEG-*b*-PNVCL (Fig. 10b). Data indicate negligible cytotoxicity of the GNR@PEG$_{114}$-*b*-PNVCL$_{237}$ against L929 cell line in the concentration range of 1-200 μg/mL, with indistinctive cell proliferation inhibition (< 10%) at high concentrations (200 μg/mL) after 72-h incubation. These results indicate excellent biocompatibility of the GNR@PEG-*b*-PNVCL for L929 cell line, suggesting the possibility of further biomedical application.
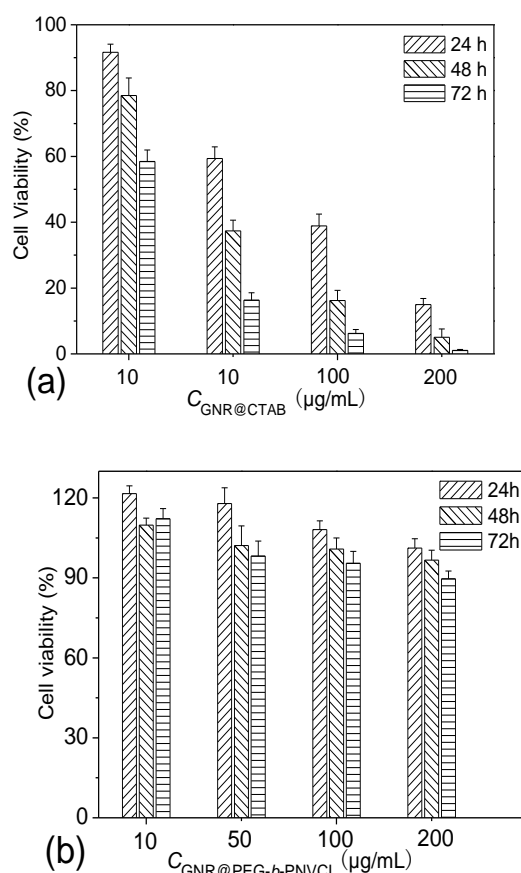

(a)

(b)

Fig. 10 Cytotoxicity profiles of GNR@CTAB (a) and GNR@PEG$_{114}$-*b*-PNVCL$_{237}$ (b) against L929 fibroblast-like cell line under different incubation concentrations and periods; percentage viabilities of the treated L929 cells were expressed relative to the untreated cells (control, 100% viability), and results were all presented as mean value ± standard deviation (n = 5).

Conclusions

Thermo-responsive poly(ethylene glycol)-*b*-poly(*N*-vinylcaprolactam) copolymers (PEG$_{114}$-*b*-PNVCL$_{25\sim237}$) were synthesized via reversible addition-fragmentation chain transfer (RAFT) polymerization of *N*-vinylcaprolactam (NVCL) from a xanthate-capped PEG macro-RAFT agent. Various well-defined PEG-*b*-PNVCL copolymers with different PNVCL lengths were successfully prepared. Their thermo-responsiveness in water was deeply investigated, and T_c of the copolymers could be tuned by modulating the length of PNVCL block. PEG$_{114}$-*b*-PNVCL$_{237}$ copolymer with a T_c of 39 °C was then used to form a thermo-responsive polymer corona over the gold nanorods (GNRs), with the xanthate end-group immobilized on the GNRs surface. We have evidenced that these GNR@PEG-*b*-PNVCL nanoparticles remain stable above the T_c of PNVCL block resulting from the stabilization effect of the hydrophilic PEG corona. Thermo-induced red-shift in the longitudinal SPR band was confirmed for the GNR@PEG-*b*-PNVCL with a good reversibility, allowing the possible application for bio-sensing. External heating and NIR-induced internal heating could trigger the pre-loaded Rhodamine® B. Importantly, faster release was observed using NIR irradiation due to a higher local overheating, compared with the conventional heating at the temperature. MTS assay disclosed that the GNR@PEG-*b*-PNVCL showed low cytotoxicity compared to those GNRs stabilized with CTAB surfactants. With all these advantages, these GNR@PEG-*b*-PNVCL nanoparticles are promising DDS platforms for chemotherapeutic and phototherapeutic functions, but also for remotely-trigger drug release under NIR laser activation.

Acknowledgements

Notes and references

^{a} Center for Education and Research on Macromolecules (CERM), University of Liege, B6 Sart Tilman, B-4000 Liège, Belgium. Fax: (32)4-36663497; Tel: (32)4-3663565; christophe.detrembleur@ulg.ac.be, c.jerome@ulg.ac.be
^{b} Laboratory of Mammalian Cell Culture (GIGA-R), University of Liège, B6 Sart Tilman, B-4000 Liege, Belgium
^{c} CNRS, Univ. Bordeaux, ICMCB, UPR 9048, F-33600 Pessac, France Fax: +33 540 002 761, Tel: +33 540 002 651, duguet@icmcb.u-bordeaux1.fr

† Electronic Supplementary Information (ESI) available: TEM image of gold nanorods before coating, schematic illustration of the apparatus for the NIR-induced heating experiment, UV/vis spectra, DLS pattern, XRD pattern, FTIR spectra of the GNR@PEG-b-PNVCL nanoparticles, NIR-induced heating profiles of GNR@PEG-b-PNVCL under irradiation (802 nm, 150 mW) and PBS buffer under different irradiation powers . See DOI: 10.1039/b000000x/

1. N. Fomina, J. Sankaranarayanan and A. Almutairi, *Adv Drug Deliv Rev*, 2012, **64**, 1005-1020.
2. E. Boisselier and D. Astruc, *Chem Soc Rev*, 2009, **38**, 1759-1782.
3. M. Tréguer-Delapierre, J. Majimel, S. Mornet, E. Duguet and S. Ravaine, *Gold Bull*, 2008, **41**, 195-207.
4. J. Xiao and L. Qi, *Nanoscale*, 2011, **3**, 1383-1396.
5. A. M. Alkilany, L. B. Thompson, S. P. Boulos, P. N. Sisco and C. J. Murphy, *Adv Drug Deliv Rev*, 2012, **64**, 190-199.
6. A. M. Alkilany, S. E. Lohse and C. J. Murphy, *Acc Chem Res*, 2012.
7. A. Llevot and D. Astruc, *Chem Soc Rev*, 2012, **41**, 242-257.
8. W. J. Mulder, G. J. Strijkers, G. A. van Tilborg, D. P. Cormode, Z. A. Fayad and K. Nicolay, *Acc Chem Res*, 2009, **42**, 904-914.
9. X. Huang, P. K. Jain, I. H. El-Sayed and M. A. El-Sayed, *Lasers Med Sci*, 2008, **23**, 217-228.
10. E. C. Dreaden, M. A. Mackey, X. Huang, B. Kang and M. A. El-Sayed, *Chem Soc Rev*, 2011, **40**, 3391-3404.
11. S. S. Huang, P. P. Yang, Z. Y. Cheng, C. X. Li, Y. Fan, D. Y. Kong and J. Lin, *J Phys Chem C*, 2008, **112**, 7130-7137.
12. E. Duguet, S. Vasseur, S. Mornet and J. M. Devoisselle, *Nanomedicine*, 2006, **1**, 157-168.
13. A. Mukerjee, A. P. Ranjan and J. K. Vishwanatha, *Curr Med Chem*, 2012, **19**, 3714-3721.
14. B. Nikoobakht and M. A. El-Sayed, *Chem Mater*, 2003, **15**, 1957-1962.
15. D. K. Kirui, D. A. Rey and C. A. Batt, *Nanotechnology*, 2010, **21**, 105105.
16. B. Van de Broek, N. Devoogdt, A. D'Hollander, H. L. Gijs, K. Jans, L. Lagae, S. Muyldermans, G. Maes and G. Borghs, *ACS Nano*, 2011, **5**, 4319-4328.
17. G. Bisker, D. Yeheskely-Hayon, L. Minai and D. Yelin, *J Control Release*, 2012, **162**, 303-309.
18. M. Chu, J. Peng, J. Zhao, S. Liang, Y. Shao and Q. Wu, *Biomaterials*, 2012. **3**, 1820-2832.
19. X. Huang, I. H. El-Sayed, W. Qian and M. A. El-Sayed, *J Am Chem Soc*, 2006, **128**, 2115-2120.
20. J. Chen, D. Wang, J. Xi, L. Au, A. Siekkinen, A. Warsen, Z. Y. Li, H. Zhang, Y. Xia and X. Li, *Nano Lett*, 2007, **7**, 1318-1322.
21. R. S. Norman, J. W. Stone, A. Gole, C. J. Murphy and T. L. Sabo-Attwood, *Nano Lett*, 2008, **8**, 302-306.
22. J. Nam, N. Won, H. Jin, H. Chung and S. Kim, *J Am Chem Soc*, 2009, **131**, 13639-13645.
23. G. von Maltzahn, A. Centrone, J. H. Park, R. Ramanathan, M. J. Sailor, T. A. Hatton and S. N. Bhatia, *Adv Mater*, 2009, **21**, 3175-3180.
24. C. Ungureanu, R. Kroes, W. Petersen, T. A. Groothuis, F. Ungureanu, H. Janssen, F. W. van Leeuwen, R. P. Kooyman, S. Manohar and T. G. van Leeuwen, *Nano Lett*, 2011, **11**, 1887-1894.
25. A. Agarwal, M. A. Mackey, M. A. El-Sayed and R. V. Bellamkonda, *ACS Nano*, 2011, **5**, 4919-4926.
26. Z. Y. Na Li , Wei Pan , Yaoyao Han , Tingting Zhang , and Bo Tang, *Adv Funct Mater*, 2012, **23**, 2255-2262..
27. S. Shen, H. Tang, X. Zhang, J. Ren, Z. Pang, D. Wang, H. Gao, Y. Qian, X. Jiang and W. Yang, *Biomaterials*, 2013, **34**, 3150-3158.
28. C. C. Chen, Y. P. Lin, C. W. Wang, H. C. Tzeng, C. H. Wu, Y. C. Chen, C. P. Chen, L. C. Chen and Y. C. Wu, *J Am Chem Soc*, 2006, **128**, 3709-3715.
29. G. Wu, A. Mikhailovsky, H. A. Khant, C. Fu, W. Chiu and J. A. Zasadzinski, *J Am Chem Soc*, 2008, **130**, 8175-8177.
30. Z. Zhang, L. Wang, J. Wang, X. Jiang, X. Li, Z. Hu, Y. Ji, X. Wu and C. Chen, *Adv Mater*, 2012, **24**, 1418-1423.
31. G. Han, C. C. You, B. J. Kim, R. S. Turingan, N. S. Forbes, C. T. Martin and V. M. Rotello, *Angew Chem Int Ed*, 2006, **45**, 3165-3169.
32. J. Liu, C. Detrembleur, B. Grignard, M. C. De Pauw-Gillet, S. Mornet, E. Duguet and C. Jerome, *Chem Asian J*, 2013, DOI: 10.1002/asia.201301010, in press.
33. R. Huschka, A. Barhoumi, Q. Liu, J. A. Roth, L. Ji and N. J. Halas, *ACS Nano*, 2012, **6**, 7681-7691.
34. T. R. Kuo, V. A. Hovhannisyan, Y. C. Chao, S. L. Chao, S. J. Chiang, S. J. Lin, C. Y. Dong and C. C. Chen, *J Am Chem Soc*, 2010, **132**, 14163-14171.
35. G. Moad, E. Rizzardo and S. H. Thang, *Polym Int*, 2010, **60**, 9-25.

36. M. I. Gibson and R. K. O'Reilly, *Chem Soc Rev*, 2013. DOI: 10.1039/C3CS60035A, in press.

37. C. A. Fustin, C. Colard, M. Filali, P. Guillet, A. S. Duwez, M. A. Meier, U. S. Schubert and J. F. Gohy, *Langmuir*, 2006, **22**, 6690-6695.

38. M. Beija, J. D. Marty and M. Destarac, *Chem Commun*, 2011, **47**, 2826-2828.

39. S. Sistach, M. Beija, V. Rahal, A. Brulte, J. D. Marty, M. Destarac and C. Mingotaud, *Chem Mater*, 2010, **22**, 3712-3724.

40. M. Beija, E. Palleau, S. Sistach, X. G. Zhao, L. Ressier, C. Mingotaud, M. Destarac and J. D. Marty, *J Mater Chem*, 2012, **20**, 9433-9442.

41. M. Liang, I. C. Lin, M. R. Whittaker, R. F. Minchin, M. J. Monteiro and I. Toth, *ACS Nano*, 2010, **4**, 403-413.

42. T. Kawano, Y. Niidome, T. Mori, Y. Katayama and T. Niidome, *Bioconjugate Chem*, 2009, **20**, 209-212.

43. A. Aqil, H. J. Qiu, J. F. Greisch, R. Jerome, E. De Pauw and C. Jerome, *Polymer*, 2008, **49**, 1145-1153.

44. R. Contreras-Caceres, A. Sanchez-Iglesias, M. Karg, I. Pastoriza-Santos, J. Perez-Juste, J. Pacifico, T. Hellweg, A. Fernandez-Barbero and L. M. Liz-Marzan, *Adv Mater*, 2008, **20**, 1666-1670.

45. A. Shiotani, Y. Akiyama, T. Kawano, Y. Niidome, T. Mori, Y. Katayama and T. Niidome, *Bioconjugate Chem*, 2010, **21**, 2049-2054.

46. B. Nikoobakht and M. A. El-Sayed, *Langmuir*, 2001, **17**, 6368-6374.

47. O. F. Solomon, D. S. Vasilescu and V. Tararescu, *J Appl Polym Sci*, 1969, **13**, 1-7.

48. M. Hurtgen, J. Liu, A. Debuigne, C. Jerome and C. Detrembleur, *J Polym Sci Polym Chem*, 2012, **50**, 400-408.

49. A. Kermagoret, C. A. Fustin, M. Bourguignon, C. Detrembleur, C. Jérôme and A. Debuigne, *Polym Chem*, 2013, **4**, 2575-2583.

50. L. D. Shao, M. Q. Hu, L. Chen, L. Xu and Y. M. Bai, *Reactive Funct Polym*, 2012, **72**, 407-413.

51. A. Debuigne, J. R. Caille and R. Jerome, *Angew Chem Int Edit*, 2005, **44**, 1101-1104.

52. A. Debuigne, R. Poli, C. Jerome, R. Jerome and C. Detrembleur, *Prog Polym Sci*, 2009, **34**, 211-239.

53. M. Hurtgen, C. Detrembleur, C. Jerome and A. Debuigne, *Polym Rev*, 2011, **51**, 188-213.

54. D. C. Wan, Q. Zhou, H. T. Pu and G. J. Yang, *J Polym Sci Polym Chem*, 2008, **46**, 3756-3765.

55. Y. C. Yu, U. H. Kang and J. H. Youk, *Colloid Polym Sci*, 2012, **290**, 1107-1113.

56. Y. M. Bai, C. X. Yan, L. D. Shao, Y. F. Wang, Y. G. Ma and G. Tang, *J Polym Sci Polym Chem*, 2013, **51**, 3240-3250.

57. J. Liu, C. Detrembleur, M. Hurtgen, A. Debuigne, M. C. De Pauw-Gillet, S. Mornet, E. Duguet and C. Jerome, Polym Chem, 2013, DOI: 10.1039/C1033PY00839H, in press.

58. Y. Kotsuchibashi, Y. Kuboshima, K. Yamamoto and T. Aoyagi, *J Polym Sci Polym Chem*, 2008, **46**, 6142-6150.

59. A. Glaria, M. Beija, R. Bordes, M. Destarac and J. D. Marty, *Chem Mater*, 2013, **25**, 1868-1876.

60. S. Slavin, A. Soeriyadi, L. Voorhaar, M. R. Whittaker, C. R. Becer, C. Boyer, T. P. Davis and D. M. Haddleton, *Soft Matter*, 2012, **8**, 118-128.

61. X. H. Li, Y. C. Li, Y. W. Tan, C. H. Yang and Y. F. Li, *J Phys Chem B*, 2004, **108**, 5192-5199.

62. Y. Fang, W. S. Chang, B. Willingham, P. Swanglap, S. Dominguez-Medina and S. Link, *ACS Nano*, 2012, **6**, 7177-7184.

63. C. J. Orendorff and C. J. Murphy, *J Phys Chem B*, 2006, **110**, 3990-3994.

64. S. Mornet, S. Vasseur, F. Grasset and E. Duguet, *J Mater Chem*, 2004, **14**, 2161.

65. S. Mornet, S. Vasseur, F. Grasset, P. Veverka, G. Goglio, A. Demourgues, J. Portier, E. Pollert and E. Duguet, *Prog Solid State Chem*, 2006, **34**, 237-247.

66. J. E. Wong, A. K. Gaharwar, D. Muller-Schulte, D. Bahadur and W. Richtering, *J Colloid Interface Sci*, 2008, **324**, 47-54.

67. S. Louguet, B. Rousseau, R. Epherre, N. Guidolin, G. Goglio, S. Mornet, E. Duguet, S. Lecommandoux and C. Schatz, *Polym Chem*, 2012, **3**, 1408-1417.

68. J. Liu, C. Detrembleur, A. Debuigne, M. C. De Pauw-Gillet, S. Mornet, L. Vander Elst, S. Laurent, C. Labrugere, C. Jerome and E. Duguet, *Nanoscale*, 2013, DOI: 10.1039/C3NR02861E, in press.

69. A. P. Leonov, J. Zheng, J. D. Clogston, S. T. Stern, A. K. Patri and A. Wei, *ACS Nano*, 2008, **2**, 2481-2488.

70. C. Shobhit, K. Sanjiv, N. Singh, F. C. Chien, Y. F. Chen, N. Nergui, S. H. Huang, C. W. Kuo, T. C. Lee and P. Chen, *Bioconjugate Chem*, 2012. **23**, 2173–2182.

Graphical abstract

GNRs with CTAB bilayers

RB

NIR
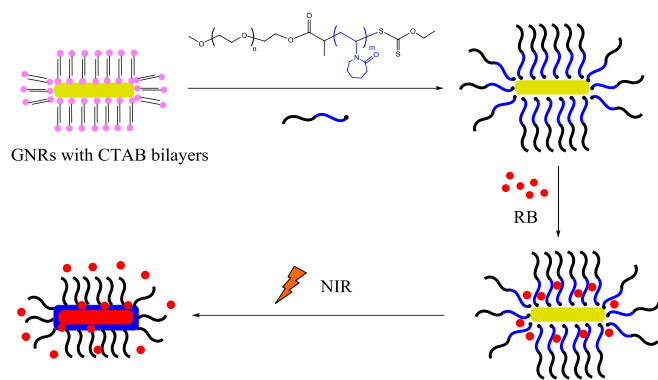
Scheme: Preparation of GNR@PEG-*b*-PNVCL, guest loading of Rhodamine® B (RB) and remotely triggered release of RB by near infrared (NIR) activation